Inorganic Chemistry

Article

pubs.acs.org/IC

Structure and Bonding of Bi_4Ir: A Difficult-to-Access Bismuth Iridide with a Unique Framework Structure

Anna Isaeva,[†] Michael Ruck,*[,†,‡] Konrad Schäfer,[§] Ute Ch. Rodewald,[§] and Rainer Pöttgen*[,§]

[†]Department of Chemistry and Food Chemistry, Technische Universität Dresden, 01062 Dresden, Germany

[‡]Max Planck Institute for Chemical Physics of Solids, Nöthnitzer Straße 40, 01187 Dresden, Germany

[§]Institut für Anorganische und Analytische Chemie, Universität Münster, Corrensstraße 36, 48149 Münster, Germany

Supporting Information

ABSTRACT: Crystals of Bi_4Ir, a new intermetallic compound, were obtained by the reaction of an iridium-containing intermetallic precursor with liquid bismuth. X-ray diffraction on a single crystal revealed a rhombohedral structure [$R\bar{3}m$, a = 2656.7(2) pm, and c = 701.6(4) pm]. Bi_4Ir is not isostructural to Bi_4Rh but combines motifs of the metastable superconductor $Bi_{14}Rh_3$ with those found in the weak topological insulator $Bi_{14}Rh_3I_9$. The two crystallographically independent iridium sites in Bi_4Ir have square-prismatic and skewed-square-antiprismatic bismuth coordination with Bi−Ir distances of 283−287 pm. By sharing common edges, the two types of [$IrBi_8$] units constitute a complex three-dimensional network of rings and helices. The bonding in the heterometallic framework is dominated by pairwise Bi−Ir interactions. In addition, three-center bonds are found in the bismuth triangles formed by adjacent [$IrBi_8$] polyhedra. Density functional theory based band-structure calculations suggest metallic properties.

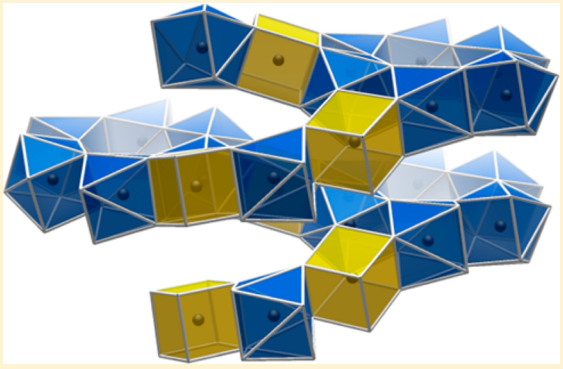

INTRODUCTION

The synthesis of bismuth-rich intermetallic compounds of high-melting transition metals is strongly hampered by the dramatic differences between the boiling point of bismuth (1883 K) and the much higher melting points of the transition metals, e.g., 2683 K for iridium or 2239 K for rhodium.[1] Only small amounts of rhodium and iridium are soluble in liquid bismuth, and flux synthesis is slow. Early investigations of the Bi−Ir system by melt reactions and subsequent annealing yielded the binary phases Bi_2Ir and Bi_3Ir.[2,3] The structure types β-Bi_2Rh and Bi_3Ni were assigned on the basis of Debye−Scherrer diffractograms. Subsequent studies by Kjekshus[4] could not reproduce Bi_2Ir either by annealing experiments or by chemical-transport reactions. Phase-pure Bi_2Ir nanoparticles were only recently synthesized via a microwave-assisted polyol process.[5] Bi_2Ir is a weakly paramagnetic semimetal. Bi_3Ir nanoparticles can be obtained by the same technique;[6] these nanoparticles reversibly intercalate oxygen up to the composition Bi_3IrO_2.[7] The latter material appears to be a unique metallic oxide ion conductor and is also the first one that operates at room temperature.

Single crystals of $Bi_3(Ir_{0.77}Cu_{0.17}Ni_{0.06})$ were recently obtained from intermetallic precursor compounds.[7] In metal flux synthesis, the broadly applied approach to intermetallics,[8−10] bismuth has only scarcely been used for the growth of phosphides and germanides. Recent examples include $Lu_3Ir_7P_5$,[11] $ScRh_6P_4$,[12] $CeRh_6Ge_4$,[13] and $Ce_2Rh_3Ge_5$.[14] In the pursuit of expanding our explorative bismuth flux technique to ternary antimonides, we have repeatedly obtained crystals of binary bismuth−iridium phases as byproducts. The crystal structure and chemical-bonding peculiarities of the hitherto unknown bismuth-richest phase, Bi_4Ir, are reported herein.

EXPERIMENTAL SECTION

Synthesis. Single crystals of Bi_4Ir are accessible from the reaction of an iridium-containing intermetallic precursor with liquid bismuth. In a typical experiment, a sample of the nominal composition $Sm_3Ir_3Sb_7$ was synthesized by arc-melting[15] from the elements [samarium pieces (Smart Elements), iridium powder (Allgemeine Pforzheim), and antimony lumps (Johnson Matthey), all with purities >99.9%] under 700 mbar of argon (purified with titanium sponge at 900 K, with silica gel, and with molecular sieves). The crushed $Sm_3Ir_3Sb_7$ regulus was subsequently mixed with 40 mol equiv of bismuth shots (ABCR; >99.9%). The mixture was placed in a corundum crucible, which afterward was sealed in an evacuated silica tube. The ampule was rapidly heated up to 1370 K in a muffle furnace and kept at that temperature for 1 week. Then the temperature was decreased to 1070 K by radiative heat loss, and the sample was annealed at that temperature for another 1 week, followed by slow cooling to room temperature within 60 h. The bismuth excess was slowly dissolved in an equimolar solution of H_2O_2 (Acros; 35%) and glacial acetic acid (VWR International). The resultant sample was washed with demineralized water. The reaction products were SmSb, elemental

Special Issue: To Honor the Memory of Prof. John D. Corbett

Received: September 11, 2014
Published: October 22, 2014

   dx.doi.org/10.1021/ic502205k | Inorg. Chem. 2015, 54, 885−889

iridium, Bi_3Ir, and Bi_4Ir as well as thin fibers of a samarium−iridium antimonide−bismuthide with an approximate composition $SmIrSb_5Bi_2$ [energy-dispersive X-ray (EDX) data].[16] Various phases were easily separated from each other mechanically based on their crystal habits.

Certainly, the synthesis of Bi_4Ir was not targeted in the way presented. We repeatedly observed Bi_4Ir from bismuth flux experiments on related ternary antimonides. These data underline that Bi_4Ir is achievable and reproducible through this technique. This does, however, not mean that such a strategy can generally by applied to related binaries.

EDX Analyses. The composition of the Bi_4Ir crystals was analyzed by EDX using a ZEISS EVO MA10 scanning electron microscope in variable pressure mode. Elemental iridium and bismuth were used as standards. No impurity elements heavier than sodium (detection limit of the instrument) were observed. The crystals exhibited the composition of 80 ± 1 atom % bismuth and 20 ± 1 atom % iridium, in excellent agreement with the proposed formula Bi_4Ir.

Single-Crystal X-ray Diffraction. Small block-shaped single crystals of Bi_4Ir were isolated from the flux by mechanical fragmentation. In order to check the crystal quality, Laue photographs of the crystals were collected on a Buerger precession camera (white molybdenum radiation, imaging plate technique, and Fujifilm BAS-1800). Intensity data were collected at room temperature using a Stoe IPDS-II imaging plate diffractometer (graphite-monochromatized Mo Kα radiation; λ = 71.073 pm) in the oscillation mode. Numerical absorption correction (μ = 131.2 mm^{-1}) was applied to the data set. Lattice metrics and systematic reflection conditions first suggested the monoclinic space groups *C*2/*m*, *Cm*, and *C*2. The centrosymmetric group was chosen for the first structure refinement. The starting atomic parameters were found by means of the *SUPERFLIP* program,[17] implemented in the *JANA2006* package.[18] Critical inspection of the resultant structure model gave strong hints for higher, presumably rhombohedral, symmetry. Evaluation of the monoclinic structural model with the *PLATON* routine[19] readily led to the correct space group, $R\bar{3}m$. Examples of overlooked trigonal symmetry are well-known for diverse structures.[20] The setting obtained for Bi_4Ir from *PLATON* was subsequently standardized with the *TIDY* routine,[21,22] and the structure refinement has smoothly converged to the residuals listed in Table 1. The final positional parameters and interatomic distances are listed in Tables 2 and 3. All sites are fully occupied. Further details on the structure determination are available from Fachinformationszentrum Karlsruhe, D-76344 Eggenstein-Leopoldshafen, Germany, by quoting CSD 428458.

Quantum-Chemical Calculations. Scalar-relativistic and fully relativistic density functional theory (DFT)-based calculations were performed using the full-potential linearized augmented plane wave (LAPW) method[23] within the local density approximation. Chemical bonding was characterized via topological analysis of the real-space electron localizability indicator (ELI-D, γ^{σ}_{D})[24,25] that was performed in the *DGrid* program package[26] and visualized with the *Paraview* software.[27] Formal atomic charges were calculated via integration of the electron density (ρ) in basins according to the quantum theory of atoms in molecules (QTAIM) developed by Bader.[28]

RESULTS AND DISCUSSION

Synthesis and Structure. The fundamental obstacles that hamper direct crystal growth of bismuth−iridium phases have been ameliorated by activating iridium via a prereaction with antimony and samarium with the subsequent addition of bismuth to the system. The Bi_4Ir crystals are one of the reaction products (see the Experimental Section) that grew out of the quaternary reaction mixture. The formation of byproducts cannot be avoided, and pure-phase samples cannot be synthesized by this method.

As by now, Bi_4Ir represents the bismuth-richest phase in the Bi−Ir system. Bi_4Ir is not isostructural to Bi_4Rh[29,30] but crystallizes in a novel rhombohedral structure type with 18 formula units per unit cell [$R\bar{3}m$, a = 2656.7(2) pm, and c = 701.6(4) pm]. Although the structure features a large unit cell, it is built by only two simple building units. The coordination spheres of two nonequivalent iridium atoms are constituted by eight bismuth atoms each. The Ir2-centered polyhedron is a slightly elongated cube (a square prism), while the Ir1-centered one is a skewed square antiprism (square faces are rotated by 31°). The Bi−Ir distances fall in the narrow range from 283 to 287 pm. They are somewhat longer than those in Bi_3Ir (276−279 pm)[7] or than the sum of the covalent radii (278 pm).[1] The cubes and antiprisms occur in the ratio 1:2 and form a complex three-dimensional network $^{3}_{\infty}[IrBi_{8/2}]$ by sharing common edges (Figures 1 and 2).

Cubic or square-antiprismatic coordination of electron-rich transition-metal atoms (M) by bismuth atoms is found in various bismuth-rich binary and ternary compounds. Solely skewed cubes (square faces rotated by 19°) are reported for the structure of α-Bi_4Rh.[29,30] Cubes and antiprisms in the ratio 2:1 constitute the isomorphous polyhedral networks of the metastable intermetallic compound $Bi_{14}Rh_3$[31,32] as well as of the subhalides $Bi_{12}Rh_3Cl_2$[32] and $Bi_{12}Rh_3Br_2$.[33] The intermetallic honeycomb layers in $Bi_{14}Rh_3I_9$,[34,35] $Bi_{13}Pt_3I_7$,[36,37] and $Bi_{12}Pt_3I_5$[37] are formed entirely by $[MBi_{8/2}]$ cubes. In all of the aforementioned cases, the local connectivity is the same. Each polyhedron is linked to four others, defining two trigonal prisms of bismuth atoms; i.e., there are two trigonal prisms per three polyhedra.

The polyhedral network of Bi_4Ir combines structural motifs that resemble those in the topological insulator $Bi_{14}Rh_3I_9$ (six-membered rings of polyhedra stacked along 0, 0, z) with those found in the superconductor $Bi_{14}Rh_3$ (helices of alternating cubes and antiprisms around $^1/_3$, $^1/_3$, z and, with opposite

Table 1. Crystal Data and Structure Refinement for Bi_4Ir

empirical formula	Bi_4Ir
cryst syst	trigonal, rhombohedral
space group	$R\bar{3}m$
Pearson symbol	*hR*135
fw, g mol^{-1}	1028.1
unit cell dimensions, pm	a = 2656.7(2), c = 701.6(4)
cell volume, nm^3	V = 4.2881
formula units per cell	Z = 27
calcd density, g cm^{-3}	10.75
diffractometer type	IPDS-II
detector distance, mm	60
exposure time, min	3
ω range; increment, deg	0−180, 1.0°
integration param (A, B, EMS)	13.3, 3.1, 0.013
cryst size, μm^3	20 × 20 × 60
abs coeff, mm^{-1}	131.2
transmn ratio (max/min)	3.54
F(000), e	11043
θ range for data collection, deg	3−30
range in *hkl*	±36, ±36, ±8
total no. of reflns	5339
indep reflns/R_{int}	959/0.088
reflns with $I \geq 2\sigma(I)/R_{\sigma}$	477/0.120
no. of data/param	959/41
GOF on F^2	0.74
R1/wR2 for $I > 2\sigma(I)$	0.028/0.044
R1/wR2 (all data)	0.058/0.092
extinction coeff	38(8) × 10^{-5}
largest diff peak/hole (e Å^{-3})	5.84/−5.17

dx.doi.org/10.1021/ic502205k | Inorg. Chem. 2015, 54, 885−889

Table 2. Atomic Coordinates and Anisotropic Displacement Parameters (pm^2) for Bi_4Ir[a]

atom	site	x	y	z	U_{11}	U_{22}	U_{33}	U_{12}	U_{13}	U_{23}	U_{eq}
Bi1	36*i*	0.06061(4)	0.24008(4)	0.18365(13)	133(4)	131(4)	147(4)	49(4)	−6(4)	20(4)	145(3)
Bi2	36*i*	0.13027(5)	0.38324(4)	0.03919(15)	229(5)	106(4)	195(5)	60(4)	−80(4)	−17(4)	187(4)
Bi3	18*h*	0.60481(3)	−*x*	0.0325(2)	129(4)	U_{11}	179(7)	53(5)	−14(3)	$-U_{13}$	151(4)
Bi4	18*h*	0.75189(3)	−*x*	0.08165(19)	177(5)	U_{11}	131(7)	97(6)	6(3)	$-U_{13}$	158(5)
Ir1	18*g*	0.16937(5)	0	$^1/_2$	123(4)	114(6)	151(7)	57(3)	−5(3)	−10(5)	130(4)
Ir2	9*e*	$^1/_2$	0	0	135(6)	71(8)	140(9)	35(4)	−2(3)	−5(7)	122(6)

[a]The anisotropic displacement factor exponent takes the form $-2\pi^2[(ha^*)^2U_{11} + \ldots + 2hka^*b^*U_{12}]$. $U_{12} = U_{23} = 0$.

Table 3. Interatomic Distances (pm) in Bi_4Ir[a]

Bi1−Ir1 (×1)	283.2	Bi3−Ir1 (×2)	284.9
Bi1−Ir2 (×1)	286.3	Bi3−Bi1 (×2)	321.5
Bi1−Bi1 (×1)	315.8	Bi3−Bi4 (×1)	331.8
Bi1−Bi3 (×1)	321.5	Bi3−Bi4 (×2)	352.7
Bi1−Bi2 (×1)	327.0	Bi4−Ir1 (×2)	284.6
Bi1−Bi2 (×1)	344.7	Bi4−Bi2 (×2)	318.3
Bi1−Bi2 (×1)	361.5	Bi4−Bi3 (×1)	331.8
Bi1−Bi4 (×1)	379.3	Bi4−Bi3 (×2)	352.7
Bi1−Bi1 (×1)	379.7	Bi4−Bi1 (×2)	379.3
Bi2−Ir1 (×1)	284.1	Ir1−Bi1 (×2)	283.2
Bi2−Ir2 (×1)	286.9	Ir1−Bi2 (×2)	284.1
Bi2−Bi4 (×1)	318.3	Ir1−Bi4 (×2)	284.6
Bi2−Bi2 (×1)	326.0	Ir1−Bi3 (×2)	284.9
Bi2−Bi1 (×1)	327.0	Ir2−Bi1 (×4)	286.3
Bi2−Bi1 (×1)	344.7	Ir2−Bi2 (×4)	286.9
Bi2−Bi1 (×1)	361.5		
Bi2−Bi2 (×1)	369.0		

[a]All distances within the first coordination spheres are listed. Standard deviations are all equal or less than 0.2 pm.

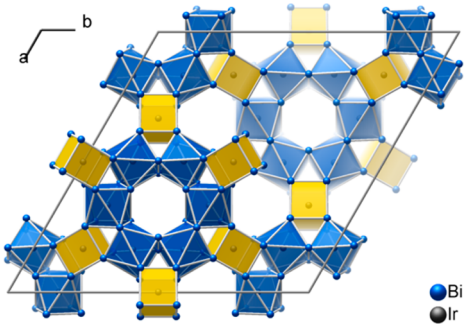

Figure 1. View of the Bi_4Ir structure along the *c* axis. The edge-sharing $[IrBi_{8/2}]$ cubes (Ir2, yellow) and square antiprisms (Ir1, blue) are emphasized.

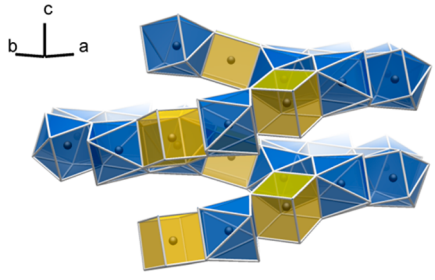

Figure 2. Cutout of the Bi_4Ir structure with edge-sharing $[IrBi_{8/2}]$ cubes (Ir2, yellow) and square antiprisms (Ir1, blue), emphasizing the mixed helix (central axis) and the attached six-membered rings of the antiprisms.

chirality, around $^2/_3$, $^2/_3$, *z*). In contrast to $Bi_{12}Rh_3X_2$ (X = Bi, Cl, and Br),[31−33] thorough analysis of the residual electron density inside the helices of the Bi_4Ir structure does not reveal any additional "interstitial" atoms X on their central axes. Likewise, the hexagonal prisms defined by six $[IrBi_8]$ cubes are not centered by isolated atoms, as has been found in the above-mentioned layered subiodides. Consistently, the inner diameters of the unfilled structural motifs in Bi_4Ir are about 50−100 pm smaller. As in all of the other structures, the lone pairs of the bismuth atoms, which decorate the surface of the framework, are pointing into these voids (cf. Figure 3 and the discussion below).

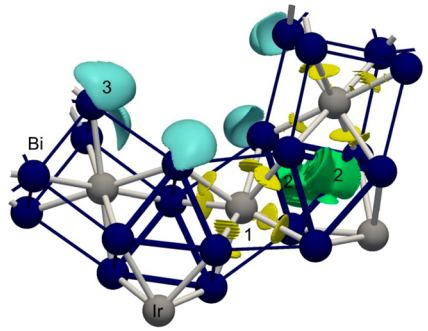

Figure 3. Fragment of the Bi_4Ir structure with both types of iridium coordination polyhedra and trigonal prisms of bismuth atoms connecting them. Thicker lines signify the strongest bonds in the framework. ELI-D localization domains given at $\gamma = 1.01$ [1, pairwise Bi−Ir bonds (0.8−0.9 electrons); 2, three-center bond slightly off the base of the trigonal prism formed by bismuth atoms (0.4 electrons)] and at $\gamma = 1.08$ [3, Bi 6s lone pairs (1.6−2.4 electrons)].

Electronic Structure and Chemical Bonding. The slightly higher electronegativity of iridium in comparison to rhodium, as evidenced by the estimated values of the ionization potentials,[38] suggests that the iridium atom in Bi_4Ir should bear a larger negative charge than the rhodium atom in Bi_4Rh. The higher electronic withdrawal toward iridium, opposite to rhodium, is further confirmed by formal atomic charges (calculated according to the QTAIM): 1.0− for iridium and 0.2+ to 0.3+ for bismuth in Bi_4Ir but 0.7− for rhodium and 0.3+ to 0.35+ for bismuth in $Bi_{14}Rh_3I_9$.[34]

Apart from monosynaptic basins, which correspond to bismuth lone pairs and closed shells or the iridium penultimate and core shells, there exist two types of ELI-D maxima that designate bonding interactions: (a) eight pairwise Bi−Ir bonds per polyhedron; (b) three-center Bi−Bi bonds that reside in the upper and lower bases of every trigonal prism defined by edge-sharing $[IrBi_8]$ polyhedra (Figure 3). The latter bonds manifest themselves also through the shorter Bi−Bi distances in the prisms (ca. 3.27 Å), as opposed to the other Bi−Bi contacts

dx.doi.org/10.1021/ic502205k | *Inorg. Chem.* 2015, 54, 885−889

within the framework (3.4−3.6 Å). The bonding pattern strongly resembles that of $Bi_{14}Rh_3I_9$,[34] in which the respective bonding basins comprise 1.1 and 0.8 electrons.[28] The corresponding electron count for Bi_4Ir yields about 0.8−0.9 and 0.4 electrons, respectively.

The conductivity pathway provided by the bonding network propagates along the entire framework and thus accounts for metallic properties predicted by the DFT-based calculations (Figures 4 and 5). Strongly mixed Ir d and Bi p states provide

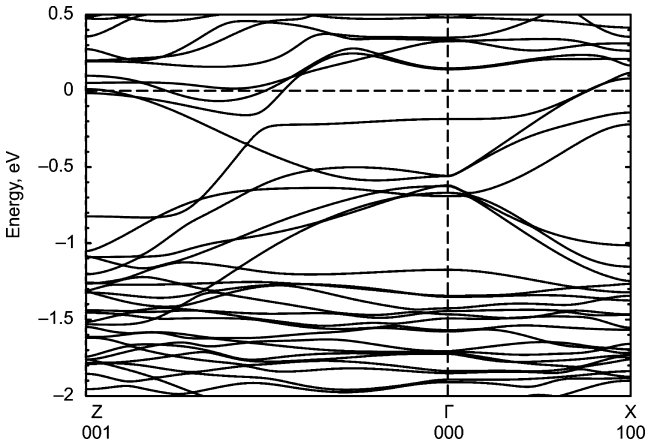

Figure 4. Band structure of Bi_4Ir in the scalar-relativistic approximation. The Fermi level resides at 0 eV.

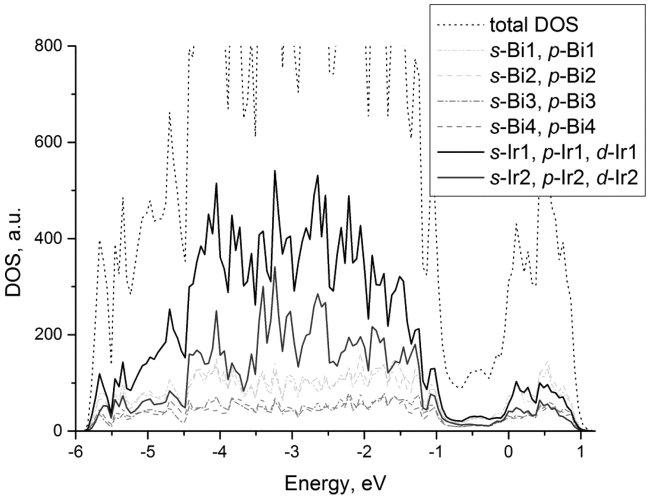

Figure 5. Total density of states and partial atomic contributions in Bi_4Ir.

the dominant contribution to the density of states at the Fermi level (Figure 5) and thus account for the metallic conductivity. Bismuth atoms that occupy various sites show no notable differences either in their contributions to bands or in their homo- and heteroatomic distances. An interesting detail of the Bi_4Ir band structure is a pseudogap that appears in the energy range between −1.0 and −0.2 eV (Figure 4) in the scalar-relativistic approximation. A gap opening under spin−orbit coupling, possibly indicating a transition in the topological state of matter,[34,39] has not been observed in the ensuing fully relativistic calculation. The spin−orbit coupling manifests itself in moderate energy splitting of the relevant bands.

CONCLUSION

The bismuth-rich intermetallic compound Bi_4Ir is accessible in the form of block-shaped single crystals from bismuth flux reactions of different quaternary Sm−Ir−Sb−Bi starting compositions. The basic building units of the Bi_4Ir structure are square-prismatic and skewed-square-antiprismatic $[IrBi_8]$ units with Ir−Bi distances of 283−287 pm, which condense to a complex three-dimensional network that is dominated by strong Ir−Bi bonding.

ASSOCIATED CONTENT

Supporting Information

Crystallographic data in CIF format. This material is available free of charge via the Internet at http://pubs.acs.org.

AUTHOR INFORMATION

Corresponding Authors

*E-mail: michael.ruck@tu-dresden.de.
*E-mail: pottgen@uni-muenster.de.

Author Contributions

The manuscript was written through contributions of all authors. All authors have given approval to the final version of the manuscript.

Notes

The authors declare no competing financial interest.

ACKNOWLEDGMENTS

This work was supported by the Deutsche Forschungsgemeinschaft.

DEDICATION

In memory of John Corbett.

REFERENCES

(1) Emsley, J. *The Elements*; Oxford University Press: Oxford, U.K., 1999.
(2) Zhuravlev, N. N.; Smirnova, E. M. *Sov. Phys. Crystallogr.* **1966**, *10*, 694−697.
(3) Massalski, T. B., Okamoto, H., Subramanian, P. R., Kacprzak, L., Eds. *Binary Alloy Phase Diagrams*, 2nd ed. (version 1.0.); ASM International: New York, 1996.
(4) Kjekshus, A. *Acta Chem. Scand.* **1971**, *25*, 411−422.
(5) Boldt, R.; Grigas, A.; Heise, M.; Herrmannsdörfer, T.; Isaeva, A.; Kaskel, S.; Köhler, D.; Ruck, M.; Skrotzki, R.; Wosnitza, J. *Z. Anorg. Allg. Chem.* **2012**, *638*, 2035−2043.
(6) Heise, M.; Ruck, M. *Z. Anorg. Allg. Chem.* **2012**, *638*, 1568.
(7) Heise, M.; Rasche, B.; Isaeva, A.; Baranov, A. I.; Ruck, M.; Schäfer, K.; Pöttgen, R.; Eufinger, J. P.; Janek, J. *Angew. Chem., Int. Ed.* **2014**, *53*, 7344−7348.
(8) Canfield, P. C.; Fisk, Z. *Philos. Mag. B* **1992**, *65*, 1117−1123.
(9) Kanatzidis, M. G.; Pöttgen, R.; Jeitschko, W. *Angew. Chem., Int. Ed.* **2005**, *44*, 6996−7023.
(10) Canfield, P. C. *Philos. Mag.* **2012**, *92*, 2398−2400.
(11) Pfannenschmidt, U.; Rodewald, U. Ch.; Pöttgen, R. *Z. Anorg. Allg. Chem.* **2010**, *636*, 314−319.
(12) Pfannenschmidt, U.; Rodewald, U. Ch.; Pöttgen, R. *Monatsh. Chem.* **2011**, *142*, 219−224.
(13) Voßwinkel, D.; Niehaus, O.; Rodewald, U. Ch.; Pöttgen, R. *Z. Naturforsch.* **2012**, *67b*, 1241−1247.
(14) Voßwinkel, D.; Pöttgen, R. *Z. Naturforsch.* **2013**, *68b*, 301−305.
(15) Pöttgen, R.; Gulden, Th.; Simon, A. *GIT Labor-Fachz.* **1999**, *43*, 133−137.
(16) Schäfer, K.; Pöttgen, R., unpublished results.

(17) Palatinus, L.; Chapuis, G. *J. Appl. Crystallogr.* **2007**, *40*, 786−790.
(18) Petříček, V.; Dušek, M.; Palatinus, L. *Z. Kristallogr.* **2014**, *229*, 345.
(19) Spek, A. L. *Acta Crystallogr., Sect. D* **2009**, *65*, 148−155.
(20) Cenzual, K.; Gelato, M. L.; Penzo, M.; Parthé, E. *Z. Kristallogr.* **1990**, *193*, 217−242.
(21) Parthé, E.; Gelato, L. M. *Acta Crystallogr., Sect. A* **1984**, *40*, 169−183.
(22) Gelato, L. M.; Parthé, E. *J. Appl. Crystallogr.* **1987**, *20*, 139−143.
(23) *The Elk FP−LAPW Code*, 2009−2014, http://elk.sourceforge.net (last access date: 1/10/2014).
(24) Kohout, M. *Faraday Discuss.* **2007**, *135*, 43−54.
(25) Kohout, M. *Int. J. Quantum Chem.* **2004**, *97*, 651−658.
(26) Kohout, M. *DGrid*, version 4.7; Max Planck Institut: Radebeul, Germany, 2013.
(27) Sandia National Labs, Kitware Inc., and Los Alamos National Labs. *Paraview: Parallel visualization application*, 2008, http://paraview.org (last access date: 1/10/2014).
(28) Bader, R. F. W. *Atoms in Molecules*; Oxford University Press, Oxford, U.K., 1990.
(29) Glagoleva, V. P.; Zhdanov, G. S. *Sov. Phys. JETP* **1956**, *3*, 155.
(30) Grin, Yu.; Wedig, U.; von Schnering, H. G. *Angew. Chem., Int. Ed. Engl.* **1995**, *34*, 1204−1206.
(31) Gu, Q. F.; Krauss, G.; Grin, Yu.; Steurer, W. *J. Solid State Chem.* **2007**, *180*, 940−948.
(32) Kaiser, M.; Rasche, B.; Ruck, M. *Angew. Chem., Int. Ed.* **2014**, *53*, 3254−3258.
(33) Ruck, M. *Solid State Sci.* **2001**, *3*, 369−375.
(34) Rasche, B.; Isaeva, A.; Ruck, M.; Borisenko, S.; Zabolotnyy, V.; Büchner, B.; Koepernik, K.; Ortix, C.; Richter, M.; van den Brink, J. *Nat. Mater.* **2013**, *12*, 422−425.
(35) Rasche, B.; Gerisch, A.; Kaiser, M.; Isaeva, A.; Van den Broek, W.; Koch, C.; Kaiser, U.; Ruck, M. *Chem. Mater.* **2013**, *25*, 2359−2364.
(36) Ruck, M. *Z. Anorg. Allg. Chem.* **1997**, *623*, 1535−1541.
(37) Kaiser, M.; Rasche, B.; Isaeva, A.; Kaiser, U.; Ruck, M. *Chem.—Eur. J.* **2014**, in press.
(38) Wu, Z. J.; Kawazoe, Y. *Chem. Phys. Lett.* **2006**, *423*, 81−86.
(39) Rasche, B.; Ruck, M.; Richter, M.; Koepernik, K.; van den Brink, J., unpublished results.